PAPER • **OPEN ACCESS**

Aerodynamic Investigation of the High-Lift Performance of a Propeller-Driven Regional Transport Aircraft with Distributed Propulsion

To cite this article: Dennis Keller 2023 *J. Phys.: Conf. Ser.* **2526** 012007

Aerodynamic Investigation of the High-Lift Performance of a Propeller-Driven Regional Transport Aircraft with Distributed Propulsion

Dennis Keller

Research Engineer, Institut für Aerodynamik und Strömungstechnik, Deutsches Zentrum für Luft- und Raumfahrt, Lilienthalplatz 7, 38108 Braunschweig, Germany

E-mail: dennis.keller@dlr.de

Abstract. Increased high-lift capabilities due to propeller slipstream, i.e. slipstream deflection, is seen to be one of the main benefits of distributed propulsion, as it may lead to a reduction in the main wing size and thus to reduced drag in cruise flight and/or reduced system weight and complexity. The presented work assesses the potential of distributed propulsion on the high-lift capabilities of a novel transport aircraft design from an aerodynamic point of view. The assessment is based on a regional propeller-driven transport aircraft designed within the European IMOTHEP project. Based on the initial aircraft design, a sensitivity study on the number of propellers and propeller positions with regards to the maximum lift coefficient under take-off conditions has been performed. Moreover, adjustments to the nacelle design and the propulsor integration have been investigated. The study indicates significant increases in the maximum effective lift coefficient in take-off of up to +42 % due to slipstream deflection. The increase is thereby strongly dependent on the number of propellers and the propeller positions.

1. Introduction

The demand for substantial CO_2 emission reductions in air traffic has led to an increasing research interest in air transport vehicles with (hybrid-) electric propulsion systems. While this type of propulsion system may introduce additional complexity and challenges, its usage also opens up the design space of aircraft configurations, in particular with respect to engine integration, due to nearly scale-free efficiency of electric motors. A promising approach to benefit from this circumstance is to distribute the propulsion along the entire wing span (DP). Besides potential positive effects on vertical tail plane size and aircraft weight due to flight mechanics and safety considerations [1], DP may also provide efficiency increases from an aerodynamic standpoint. Beneficial effects are thereby anticipated to originate from two sources with the first one being direct aero-propulsive efficiency increases during cruise flight and the second one being indirect benefits due to improved high-lift capabilities. In cruise flight, the flexibility of DP systems may allow for aircraft performance increases due to improved propulsor integration including wing tip propellers and hence shape optimization [2, 3]. A recent numerical investigation of the aero-propulsive efficiency of a short-range regional aircraft found a reduction in required propulsive power of $-2.9\,\%$ to $-3.3\,\%$ in cruise flight due to distributed propulsion exclusively based on direct aero-propulsive efficiency increases [4]. Besides these direct effects, DP systems promise increased high-lift capabilities in low speed, which in turn may yield benefits in cruise flight from wing sizing effects. With the light general aviation aircraft concept SCEPTOR, NASA tries to take advantage of this effect by utilizing high-lift propellers [5]. These propellers located along the main wing are only active in low speed and

are particularly designed to increase the axial velocity behind the propellers homogeneously while minimizing power consumption and thrust [6]. With this concept, Borer et al. achieved maximum lift coefficients of over 4 with a Fowler flap that extends throughout most of the span [5]. More recently, Beckers et al. investigated propeller-wing interactions of a distributed propulsion system and found an increase in lift generation of up to +63 % [7]. The increase was thereby highly dependent on the propeller position and the angle of attack.

In the framework of the European IMOTHEP project, the potential of lift augmentation in low speed is assessed for a novel hybrid-electric short range regional aircraft. Therefore, the dependence of the maximum effective lift coefficient (including airframe and propeller blade forces) on the number of propellers and the propeller positions was analyzed. Besides, additional effort was made to improve the propulsor integration. Due to the type of the aircraft concept, the propulsor nacelles are comparably large and therefore lead to potentially adverse effects on the aerodynamic performance in cruise flight as well as under high-lift conditions. The work on the propulsor integration design therefore considered the aero-propulsive efficiency in cruise flight as well as maximum lift capabilities in low speed. The results of both studies are presented in this paper.

2. Numerical Methods

The numerical simulations based on the Reynolds-averaged Navier-Stokes (RANS) equations have been carried out with the *DLR TAU* code [8]. The code relies on an unstructured finite volume approach for solving the RANS equations. For the present investigation, the implicit LU-SGS scheme was used for time stepping and a central scheme and second order Roe upwind scheme for the spatial discretization of the inviscid mean flow fluxes and the turbulent convective fluxes, respectively. The turbulence effects were modeled with the Spalart-Allmaras formulation (SA) [9] with vortical and rotational flow correction based on the Spalart-Shur correction [10]. In order to model the propeller effects, an actuator disk approach based on 2D blade element momentum theory is implemented in *TAU*. In this way, the local forces of the propeller are calculated based on the blade properties and the local flow conditions. Detailed information on the actuator disk implementation can be found in [11]. The actuator disk model has shown robust behavior and good results in terms of performance parameters as well as slipstream velocity distributions for various applications such as the simulations of conventional propellers [12], contra-rotating open rotors [13].

3. Basic Geometric Model

	Loop 0	Loop 1
Reference area	48.6 m^2	55.7 m^2
Half span	13.05 m	13.96 m
Aspect ratio	14.0	14.0
Sweep angle (leading edge)	0°	5.5°
Mean aerodynamic chord	2.18 m	2.08 m
Propeller diameter	2.6 m	3.0 m

Table 1. Basic aircraft parameters of the loop 0 and loop 1 configuration

The geometries investigated in the present study are derived from an overall aircraft design carried out within the IMOTHEP project [14]. The aircraft is designed for 40 passengers and a mission range of 200 *nm* when flying fully electric and 600 *nm* in hybrid mode. The present aerodynamic studies are based on two different design loop stages. The basic aircraft parameters of both stages are summarized in table 1. A propeller design was carried out within the project for the initial aircraft design [15]. The propellers are all chosen to be identical along each wing side and are all rotating in inboard-up direction. Figure 1 depicts the basic aircraft geometries of the loop 0 and loop 1 configurations.

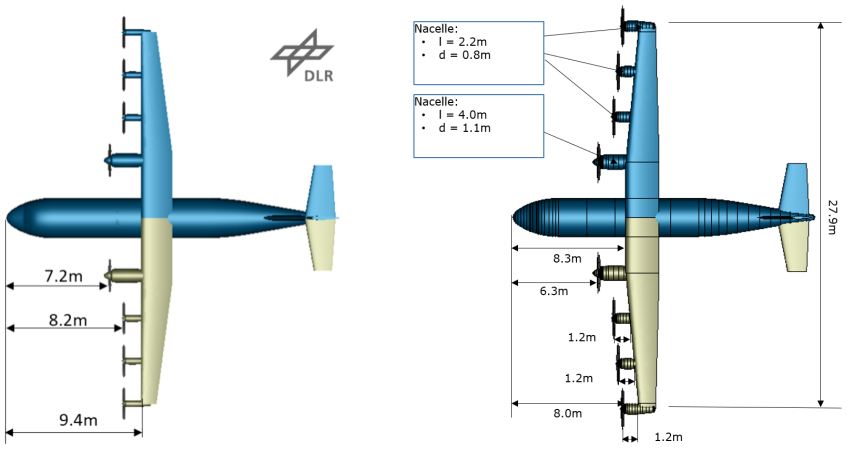

(a) Loop 0 (b) Loop 1

Figure 1. IMOTHEP overall aircraft design [14]

3.1. High-Lift System

At the beginning of the investigation, a detailed aerodynamic high-lift design has been carried out for the loop 0 configuration. The high-lift system features a single slotted drop hinge flap with a relative flap chord length of 30 % of the local chord and no leading edge device. The design was later updated for the loop 1 configuration while leaving basic design decisions such as type of systems, geometric constraints, and optimization parameters untouched.

4. Propeller Sensitivity Study

4.1. Procedure, Considerations, and Constraints

In order to assess the impact of the number of propellers and the propeller positions on the maximum effective lift coefficient under take-off conditions, 3D-RANS computations of the loop 0 take-off configuration have been carried out. In this study, the propulsor nacelles have been neglected. The parameters being varied were the streamwise position of the propellers with respect to the wing leading edge (ΔX), the vertical position of the propellers with respect to the wing leading edge (ΔZ), and the number of propellers (n). For a given number of propellers, the propeller positions with respect to the main wing leading edge are identical along the wing span. The relative spanwise distance between the propellers was kept constant at 18 % of the respective propeller diameters.

	min	max
Streamwise position ΔX	−1.5 m	−0.5 m
Vertical position ΔZ	−0.6 m	0 m
Number of propellers n	0	16

Table 2. Design constraints of sensitivity study

Table 2 summarizes the constraints of the parameters that have been varied. The limitations with regards to the streamwise position closest to the wing and in particular the vertical position have been chosen in order to prevent unrealistic propeller set ups. While varying the number of propellers, the propeller diameters have been adapted to maximize the total propeller disk area for each n with the maximum propeller diameter being $D_{prop} = 4\,m$. Therefore, the total propeller disk area obviously changes with the number of propellers, eventually impacting the blowing effect. This procedure however has been assumed to be the most realistic, as the maximization of propeller disk area leads to the optimum overall propeller efficiency in cruise flight. In order to obtain similar propeller conditions, the rotational speed of the propellers was adapted with regards to the number of propellers to achieve identical propeller

advance ratios. The propeller pitch angles were then set to achieve a total thrust of $T = 18\,kN$ (for the half model) at an angle of attack of $\alpha = 6°$ for each case. With the resulting settings, alpha sweeps were computed in order to assess the maximum effective lift coefficient for each set of parameters.

4.2. Results

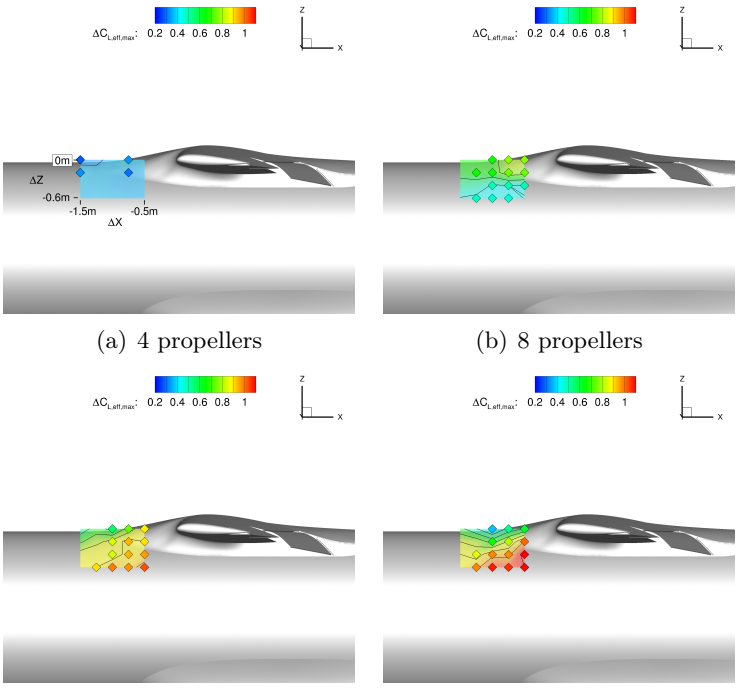

(a) 4 propellers (b) 8 propellers

(c) 12 propellers (d) 16 propellers

Figure 2. Change in maximum effective lift coefficient due to propeller slipstream effects depending on propeller position

Figure 2 visualizes the impact of the position of the propeller center on the change in the maximum effective lift coefficient ($\Delta C_{L,eff,max}$) with respect to the case with propellers off for different propeller counts. With 4 propellers (two on each wing side), the influence of the propeller position on $\Delta C_{L,eff,max}$ is rather minor (figure 2(a)). With increasing propeller count, the impact increases. With 8 propellers, the best position with regards to $\Delta C_{L,eff,max}$ appears to be close to the main wing without vertical offset (figure 2(b)). Increasing the propeller count further moves the optimum position towards a lower vertical location (figure 2(c)). Moreover, the maximum possible change in $C_{L,eff,max}$ increases. This trend is even more amplified with 16 propellers (figure 2(d)). In this case, the maximum $\Delta C_{L,eff,max}$ is achieved at $\Delta X = -0.5\,m$ and $\Delta Z = -0.4\,m$. The propeller positions for the maximum $\Delta C_{L,eff,max}$ appear to correlate with the ability to ideally enclose the main wing with the propeller slipstream at angles of attack close to α_{max}. Accordingly, the region of best propeller positions generally stretches from the lower left side towards the upper right side and decreases in width with increasing propeller count and the resulting decrease in propeller diameter.

Figure 3 compares the leading edge stagnation pressure distribution at α_{max} of the most unfavorable (red) and most favorable (green) propeller positions in the case of 16 propellers. While the leading edge stagnation pressure coefficient ($C_{p,max}$) is increased by all propeller slipstreams along the wing in the case of the most favorable propeller position, the effect of the 4 innermost propellers is marginal in the case of the most unfavorable propeller position. In this case, $C_{p,max}$ is close to the free stream stagnation pressure for $\eta \leq 0.5$. This observation also holds true for the leading edge stagnation pressure of the flaps (not shown) as it was described by Beckers et al. before [7]. The comparison confirms the hypothesis that the lift augmentation capabilities with respect to the propeller position is correlated to the ability to enclose the main wing with the propeller slipstream. It is thereby noteworthy that the behavior may differ depending on the angle of attack, in particular in the case of small propeller diameters and

respectively high propeller counts. For example, in this case, the effective lift coefficient at $\alpha = 6°$ only differs by $\Delta C_{L,eff} = 0.07$, whereas the difference at $\alpha = 11°$ is $\Delta C_{L,eff} = 0.46$. Comparing the maximum effective lift coefficient, the most unfavorable and most favorable propeller positions yield $C_{L,eff,max} = 3.09$ at $\alpha = 11°$ and $C_{L,eff,max} = 3.86$ at $\alpha = 14°$, respectively.

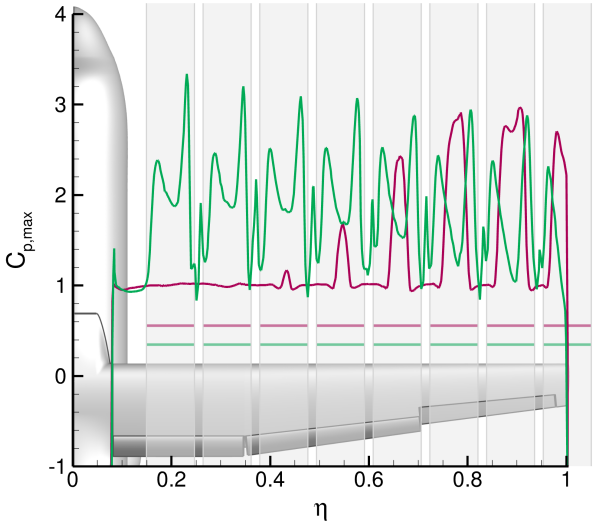

Figure 3. Comparison of leading edge stagnation pressure distribution along the main wing span at α_{max} of most unfavorable and most favorable propeller position with 16 propellers

Figure 4 depicts the maximum (effective) lift coefficients depending on the propeller count. The plot shows the results of all investigated cases with the black curve and the turquoise symbols representing the highest values achieved for each propeller count. The curves indicate a clear trend with the maximum (effective) lift coefficients increasing with rising propeller count. However, the curves flatten towards higher n. It is assumed that this behavior is (partially) caused by the rather low D_{prop}/c ratios at high propeller counts. According to Patterson et al., the effectivity of the propeller slipstream with regards to wing blowing notably decreases at low D_{prop}/c ratios [6]. With comparably high maximum (effective) lift coefficients, the cases with 2 propellers stand out. These cases do not utilize a wing tip propeller and thus the thrust is solely produced in a wing region of high base circulation mainly caused by the large local chord length and flap deployment. As a result, the propeller blowing effect is comparably large. The figure also puts the $C_{L,eff,max}$ of the initial aircraft design (red symbol) into relation with the maximum lift augmentation potential.

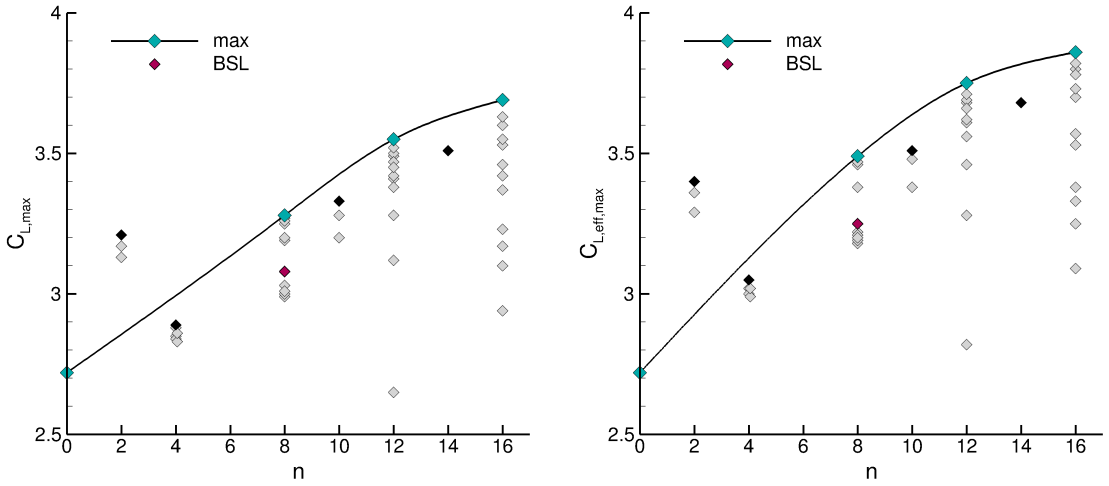

(a) maximum lift coefficient (without propeller forces)

(b) maximum effective lift coefficient (with propeller forces)

Figure 4. Maximum (effective) lift coefficient due to propeller slipstream effects depending on number of propellers

4.3. Nacelle Design

The nacelle design and propulsor integration was carried out for the loop 1 configuration at the design cruise Mach number of $M_{cr} = 0.4$ and design lift coefficient of $C_{L,MCR} = 0.7974$. Due to the integration of the electric propulsion systems, the gas turbine, batteries, and the landing gear into the nacelles, the nacelles are comparably large and lead to flow separation on the initial design. Several modifications were therefore introduced to eliminate flow separation. Figure 5 compares the surface pressure distribution, skin friction lines, and regions of flow separation (red lines) of the initial and the modified propulsor integration shape. The modification of nacelles 2 and 3 thereby yield the largest drag reduction with $\Delta C_D = -0.0016$, partly by reducing flow separation downstream of the nacelles and partly by reducing the frontal area due to a vertical repositioning of the nacelles/propellers. Additionally, the modification of nacelle 4 (tip nacelle) reduces the drag coefficient by $\Delta C_D = -0.0003$. Most effort has been spent on improving the integration of nacelle 1. Several modifications, such as decambering of the main wing downstream of the nacelle, vertical repositioning, and extending the nacelle beyond the main wing's trailing edge, have been investigated. The latter was found to be the most beneficial in cruise flight with a drag reduction of $\Delta C_D = -0.0006$. Together with additional modifications, such as twist modifications and a resulting unfavorable higher wing position, the total drag reduction sums up to $\Delta C_D = -0.0028$, yielding a decrease in required propulsive power by $-6\,\%$.

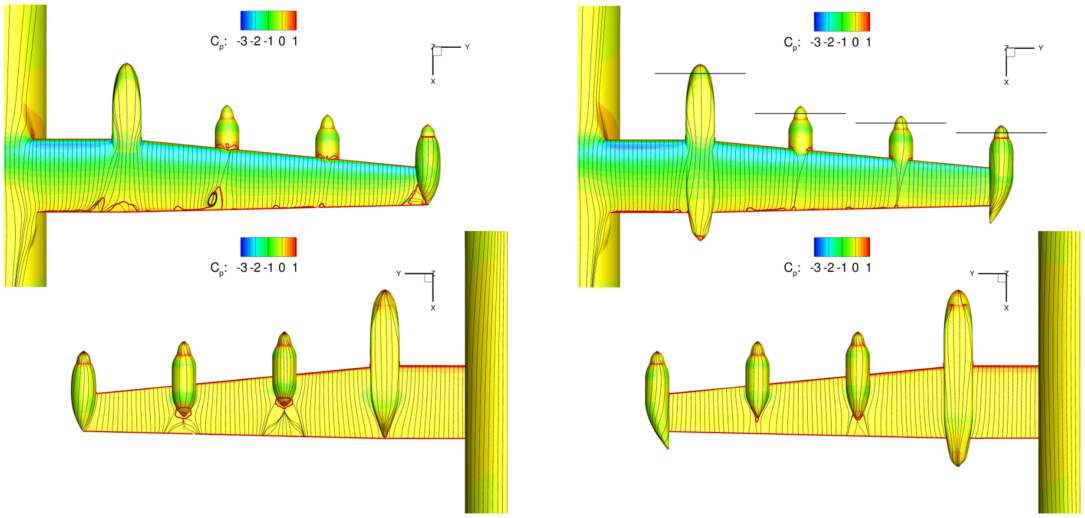

(a) initial shape (b) improved shape

Figure 5. Surface pressure distribution with skin friction lines and areas of flow separation (red lines) at cruise conditions ($M_{cr} = 0.4$, $C_{L,MCR} = 0.7974$)

The extension of nacelle 1 beyond the main wing's trailing edge obviously has an adverse effect on the high-lift performance due to the reduced high-lift device surface size. Figure 6 shows that for the take-off and the landing configuration the maximum lift coefficient is degraded due to the long nacelle 1. For both configurations with prop off condition, the reduction is $\Delta C_{L,max} = -0.1$. Considering propeller effects for the take-off configuration with maximum power condition ($484\,kW$ per propeller), the maximum effective lift coefficient is increased by $\Delta C_{L,max} = 0.62$ or $24\,\%$. In order to further enhance $C_{L,max}$ under prop off conditions, nacelle strakes have been designed for nacelle 1 and nacelle 4 based on the experience from previous studies [16]. The impact of those strakes on the flowfield of the landing configuration at high angles of attack is demonstrated in figure 7. The flowfield visualization clearly indicates delayed flow separation in proximity of nacelle 1 and nacelle 4 due to the induced strake vortices (purple

iso surfaces) in the case with nacelle strakes (figure 7(b)). As a result, $C_{L,max}$ in landing configuration is increased by 0.09 (figure 6(b)).

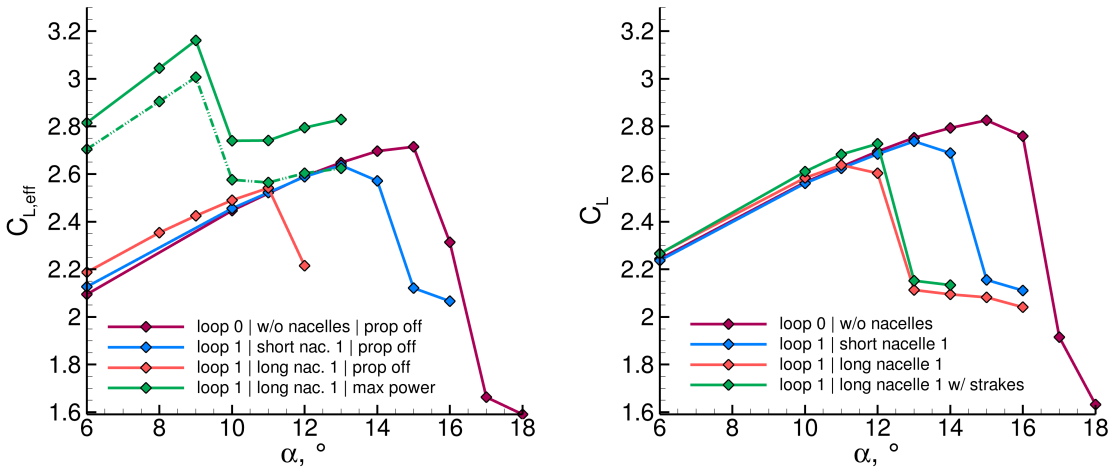

(a) take-off (b) landing

Figure 6. Lift curves of high-lift configurations

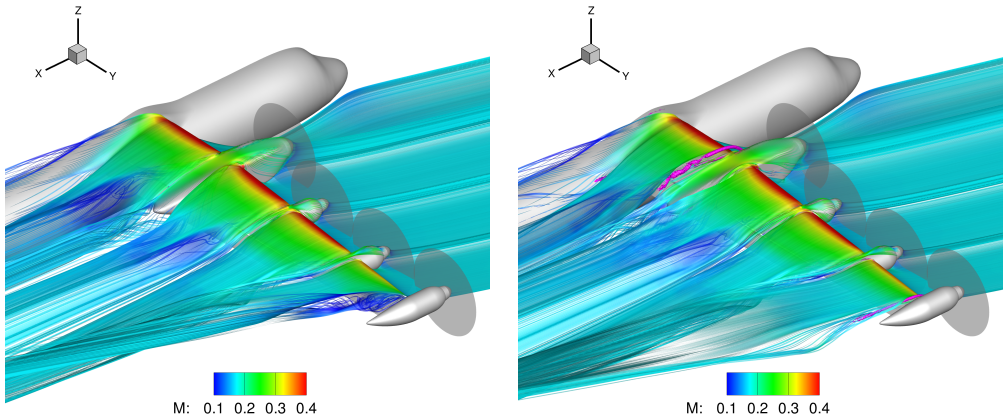

(a) without nacelle strakes (b) with nacelle strakes

Figure 7. Flow visualization in terms of streamlines colored with Mach number of loop 1 landing configuration at $\alpha = 12°$

5. Conclusions

Within the framework of the European IMOTHEP project, the aerodynamic performance of a short range regional aircraft with distributed propulsion was investigated with the focus being on the high-lift performance. In a first step, the influence of basic configurational propeller parameters on the high-lift performance under take-off conditions was assessed. The investigation demonstrates that distributed propulsion can increase the maximum effective lift by as much as $\Delta C_{L,eff,max} = 1.14$ (+42 %) due to slipstream deflection. $C_{L,eff,max}$ thereby generally increases with the number of propellers, but is highly dependent on the propeller positions. This dependency is more pronounced at small D_{prop}/c ratios, i.e. large number of

propellers. Moreover, the increase in $C_{L,eff,max}$ appears to be limited due to the D_{prop}/c ratio becoming too small and unfeasible (vertical) propeller positions.

In a second step, a numerical design study on the nacelle design and propulsor integration was carried out. The design work yielded a decrease in the drag coefficient by $\Delta C_D = -0.0028$ compared to the initial design with $\Delta C_D = -0.0006$ resulting from an nacelle extension beyond the main wing trailing edge. The extended nacelle thereby caused a reduction in the maximum lift coefficient by $\Delta C_{L,max} = -0.1$. Utilizing nacelle strakes may increase the maximum lift coefficient as it was shown for the landing configuration. Moreover, the blowing effect under take-off conditions increases in the maximum effective lift coefficient by $\Delta C_{L,eff,max} = 0.62$ or 24 % for the baseline configuration.

Acknowledgments

This project has received funding from the European Union's Horizon 2020 research and innovation program under grant agreement No. 875006 IMOTHEP.

References

[1] Biser S, Atanasov G, Hepperle M, Filipenko M, Keller D, Vechtel D, Boll M, Kastner N and Noe M 2020 Design space exploration study and optimization of a distributed turbo-electric propulsion system for a regional passenger aircraft *Proc. AIAA Propulsion and Energy 2020 Forum*

[2] Loth J and Loth F 1984 Induced drag reduction with wing tip mounted propellers *Proc. 2nd Applied Aerodynamics Conference*

[3] Sinnige T, van Arnhem N, Stokkermans T C A, Eitelberg G and Veldhuis L L M 2019 Wingtip-mounted propellers: aerodynamic analysis of interaction effects and comparison with conventional layout *Journal of Aircraft* **56** 1

[4] Keller D 2021 Towards higher aerodynamic efficiency of propeller-driven aircraft with distributed propulsion *CEAS Aeronautical Journal* **12** pp 777–91

[5] Borer K, Derlaga J M, Deere K A, Carter M B, Viken S, Patterson M D, Litherland B and Stoll A 2017 Comparison of aero-propulsive performance predictions for distributed propulsion configurations *Proc. 55th AIAA Aerospace Sciences Meeting*

[6] Patterson M D, Derlaga J M and Borer N K 2016 High-lift propeller system configuration selection for NASA's SCEPTOR distributed electric propulsion flight demonstrator *Proc. 16th AIAA Aviation Technology, Integration, and Operations Conference*

[7] Beckers M F, Schollenberger M, Lutz T, Bongen D, Radespiel R, Florenciano J L, and Funes-Sebastian E 2022 CFD investigation of high-lift propeller positions for a distributed propulsion system *Proc. AIAA AVIATION 2022 Forum*

[8] Gerhold T 2005 Overview of the hybrid RANS code TAU *MEGAFLOW – Numerical Flow Simulation for Aircraft Design, NNFM* **89** (Berlin: Springer) pp 81-92

[9] Spalart P R and Allmaras S R 1992 A one–equation turbulence model for aerodynamic–flows *Proc. 30th Aerospace Sciences Meeting and Exhibit*

[10] Spalart P R and Shur M 1997 On the sensitization of turbulence models to rotation and curvature *Aerospace Science and Technology* **1** 5 pp 297-302

[11] Raichle A 2017 Flux conservative discretization of the actuator disk model as a discontinuity surface *Ph.D. Thesis* (Braunschweig: Technical University Braunschweig)

[12] Lenfers C, Beck N and Bauer M 2016 Propeller and active high lift wing interaction in experiment and simulation *New Results in Numerical and Experimental Fluid Mechanics X* **132** (Berlin: Springer) pp 51-61

[13] Marquez Gutierrez C O, Stürmer A, Clemen C and Grimminger A 2012 Validation of actuator disk simulations of CROR propulsion systems at low-speed flight conditions *Proc. 30th AIAA Applied Aerodynamics Conference* (New Orleans, Louisiana, USA)

[14] Atanasov G 2022 IMOTHEP plug-in hybrid-electric aircraft concept: REG-RAD *12th EASN International Conf. on Innovation in Aviation and Space for opening New Horizons* (Barcelona, Spain)

[15] Maldonado Y 2022 Propeller predesign for distributed propulsion architectures *3AF - Towards sustainable aviation summit* (Toulouse, France)

[16] Keller D, Hasan Y J and Rudnik R 2018 Nacelle strake design for short takeoff and landing configuration with turboprop engines *Proc. Journal of Aircraft* **55** 6 pp 2444-53